RSC Advances

ROYAL SOCIETY OF CHEMISTRY

www.rsc.org/advances

Graphene/Nitrogen-doped Carbon Nanofiber Composite as an Anode Material for Sodium-ion Batteries

Juan Zhang, Zhian Zhang*[1], Xingxing Zhao

School of Metallurgy and Environment, Central South University, Changsha, Hunan 410083, China

Abstract

Graphene/N-doped porous carbon nanofiber (RGO/NPC) composite was designed as an anode material for sodium-ion batteries (SIBs). A microstructure of fine and uniform N-doped porous carbon nanofibers decorated on 2D RGO sheets was obtained. The RGO/NPC with larger interlayer space , the appropriate N-doped and high electrical conducitivity, combining with of the advantages of two materials, exhibits a good reversible capacity**,** including a high reversible capacity (175.9 mAh g^{-1} at 100 mA g^{-1} over 300 cycles), excellent rate capability (104 mAh g^{-1} at 1600 mA g^{-1}), and superior cycling stability (97.7 mAh g^{-1} at 1000 mA g^{-1} over 600 cycles). This new type structural material has great significance for improving the performance of SIBs.

[1] Corresponding author: Fax. & Tel: +86 731 88830649.

E-mail address:zhangzhian@csu.edu.cn (Zhian Zhang)

1. Introduction

The rareness and uneven distribution of lithium minerals can't meet the higher demands placed on lithium-ion batteries (LIBs) in the future.[1-2] Rechargeable sodium-ion batteries (SIBs) are receiving recognition as an alternative to LIBs, because of the natural abundance of Na resources, although sodium has a larger atomic mass and ionic radius (55% larger than Li^+). [3-4] A slice of ideal anode materials of LIBs exhibited very poor storage properties for SIBs, because they can barely accommodate sodium ions under moderate conditions.[5] Therefore, it is still a crucial issue to develop suitable anode materials for application in SIBs.

Many materials have been reported as anode materials for SIBs.[6-10] Among a lot of chosen materials, disordered carbon appears to be the most suitable anode materials due to the existing versatile preparation methods, relatively high electrical conductivity and the larger interlayer space for SIBs.[11] Guan *et al.*[12] reported a series of mesoporous carbons, which were obtained by pyrolyzing gelatin and magnesium citrate. Bai *et al.*[13] synthesised high-performance hard carbon from pyrolyzing polyvinyl chloride (PVC) nanofibers. Although much progress has been realized, above-mentioned carbon materials commonly obtained by using single carbon source, exhibit lower sodium storage capacity. More efforts still need to be made to improve the electrochemical performance for the commercial application of SIBs.

Graphene (RGO), a unique 2D carbon material with large surface area and excellent electronic conductivity, exhibits outstanding advantages in energy storage systems.[14] Graphene has been widely used in constructing the conducting networks for LIBs because its high electronic conductivity guarantees a high-rate capability of the electrode.[15] Nevertheless, the larger Na^+ is more difficult to insert into and extract from RGO, which has limited interlayer space for SIBs. In order to make up the shortness of RGO for SIBs, it is necessary to use other suitable material to modify the RGO. Undoubtedly, N-doped porous carbons nanofiber (NPC) should be the appropriate candidate with its larger interlayer space, appropriate N-doped and porous structure, which will facilitate good transport of electrons，accelerate absorption and intercalation of sodium ion, adequately contact to the electrolyte, and improve the electric conductivity of reversible intercalation hosts.[16-17] Wang *et al.* [18] described a 2D porous N-doped carbon sheets by chemical activation of polypyrrole (PPy)-functionalized graphene sheets with KOH, which exhibited a high reversible capacity and good rate capability. The electrochemical performance of carbonaceous anode materials for SIBs could be improved by designing nanostructures composite containing graphene nanosheets and N-doped porous carbons nanofibers.

Herein, we report on graphene/nitrogen-doped porous carbon nanofiber (RGO/NPC) composite synthesized by carbonizing graphene oxide /polyprrole nanofiber (GO/PPy) precursor for SIBs. The RGO/NPC are fully taking advantages of the high electrical conductivity of graphene and the larger interlayer space and the appropriate N-doped of NPC. Unique compositional and structural features endow the RGO/NPC with

superior SIBs performance, that is, a high reversible capacity (175.9 mAh g^{-1} at 100 mA g^{-1} over 300 cycles), an excellent rate capability(104 mAh g^{-1} at 1600 mA g^{-1}) and superior cycling stability (97.7 mAh g^{-1} at 1000 mA g^{-1} over 600 cycles), demonstrating that RGO/NPC is a appropriate and effective candidate for improving the performance of SIBs.

2. Experimental

2.1 Preparation of grapheme/nitrogen-doped porous carbon nanofiber (RGO/NPC)

To fabricate the RGO/NPC, firstly, the graphene oxide /polyprrole nanofiber (GO/PPy) was prepared as the precursor.[19] The GO/PPy was synthesized via a one-step polymerization method using pyrrole monomer and graphene oxide (GO) aqueous solution as precursors. Graphene oxide was obtained from natural graphite powder by a modified Hummers method.[20] The concentration of the as-prepared graphene oxide solution was quantified as 6.8 mg mL^{-1}. 2.82 mL of GO solution was diluted by 20 (0.1 M) of hydrochloric acid solution and then mixed with pyrrole (20 mM) and CTAB (1.5 mM) after cooling the temperature to 0~5 ^{o}C , followed by 30 min of sonication. Then 20 mM ammonium persulfate (APS) was added into the mixture and the reaction was proceeded for 24 h at 1~5 ^{o}C. The GO/PPy was obtained by filtering and washing with ethanol and deionized water. After heat treatment of the as-prepared GO and GO/PPy at 800 ^{o}C for 2 h with a heating rate of 5 ^{o}C min^{-1} under an argon atmosphere, the RGO and RGO/NPC were finally obtained.

2.2 *Material characterization*

Scanning electron microscopy (SEM, Nova SEM 230) and transmission electron microscopy (TEM, Tecnai G2 20ST) were applied to investigate the material morphology. The structure of the material was characterized using X-ray diffraction (XRD, Rigaku3014). Nitrogen adsorption/desorption measurements were performed by using Quantachrome instrument (Quabrasorb SI-3MP). Surface functional groups and bonding characterization were conducted using X-ray photoelectron spectroscopy (XPS, Thermo Fisher ESCALAB250xi). The fitting errors of XPS test results are within ± 1%.

2.3 *Electrochemical measurements*

To conduct electrochemical measurements of the RGO/NPC electrode, a CR-2025 type coin cell was fabricated. Sodium pellet and a celgard 2400 film membrane were served as counter electrode and separator, respectively. A mixed slurry of RGO/NPC, Super P and sodium alginate (SA) (8:1:1, in wt%) in deionized water was spread onto a copper foil. The coating copper foil was first dried in air, and then transferred into a oven at 80 ^{o}C for 12 h. The assembly of the tested cells was carried out in a glove box under an argon atmosphere. The electrolyte used in this work was the composition of 1 M $NaClO_4$ (Sigma-Aldrich) in a solvent mixture of ethylene carbonate (EC) and diethyl carbonate (DEC) (with a volume ratio of 1:1) with addition of 5% fluoroethylene carbonate (FEC). Galvanostatic charge/discharge test were conducted with a battery test system. Cyclic voltammetry (CV) measurements were

carried out at a scan rate of 0.2 mV s^{-1} between 0.01 and 3 V using 1470E electrochemical measurement system. Those electrochemical tests were carried out under a constant temperature of 25 ^{o}C.

3. Results and discussion

3.1 Synthesis and characterization

Fig. 1 outlines the strategy to synthesize the RGO/NPC. The RGO/NPC synthetic procedure can be divided into two steps: polymerization and carbonization. Firstly, cetrimonium bromide (CTAB) and pyrrole monomer were dispersed into the GO hydrochloric acid solution by 30 min of sonication. The concentration of CTAB was strictly controlled at 4 times its critical micelle concentration (cmc) in the polypyrrole synthesis. Under this condition, the formed micelles are wirelike.[19] When the reaction temperature was cooled to 1~5 ^{o}C, polymerization reaction occurred and the polypyrrole fibers were incorporated with the GO nanosheets to form GO/PPy, with the aid of ammonium persulfate (APS). The GO/PPy was subsequently pyrolyzed at 800 □ for 2 h under a nitrogen atmosphere, resulting in RGO/NPC with N-doped and abundant porous channels.

The morphology characterization of RGO and RGO/NPC were investigated using scanning electron microscope (SEM) and transmission electron microscope (TEM). After heat treatment of the as-prepared Go, Fig. 2a shows the appearance of 2D RGO, which the nanosheets overlap with each other and exhibit a thin, wrinkled structure, resulting in a large amount of free space between the graphene layers. [7] After being

incorporated with the NPC derived from the polypyrrole fibers, the long and tangled nanofibers are evenly distributed on the RGO nanosheets, which are coated with a very thin layer of the amorphous NPC at the same time (Fig 2b).[19] The RGO is composed of thinner transparent sheets and some thicker ripples (Fig. 2c) and will facilitate good transport of electrons. The transparency implies that the RGO nanosheets are only a few layers, the dark ripples are due to crumpling of nanosheets. [7] The structure of composite is much clearer under TEM (Fig 2d), the RGO set up the carbon skeleton and NPC are distributed or coated on the RGO. Fig. 2e-g demonstate the annular dark-field TEM images of the RGO/NPC and the corresponding elemental mapping of nitrogen and carbon. It can been observed the presence of nitrogen on the RGO, suggesting the NPC are coated on the RGO. Meanwhile, these figures reveal the presence and homogeneous distribution of nitrogen of RGO/NPC, which would result effective absorption of sodium ions.

Fig. 3(a) shows that all of the XRD patterns of the RGO, NPC and RGO/NPC composites have two broad peaks observed at around 23^{o} and 43^{o}, which can be indexed to (002) and (100) , respectively, and demonstrates that they have semblable crystalline structure. This XRD patterns indicate amorphous structure of the RGO, NPC and RGO/NPC. Based on the XRD result, the interlayer spacing (d_{002}) of CNF/NPC is 0.36 nm by calculation. The larger interlayer spacing of RGO/NPC than RGO (0.34 nm) make it a suitable host material for SIBs to store sodium ion since since sodium ion is 55% larger than lithium ion in radius. To further characterize the surface and the porous structures of the RGO/NPC, N_2 absorption-desorption

measurement was also carried out. Fig. 3(b) inset shows a typical type IV isotherm with a hysteresis loop within a relative pressure P/P_0 range of 0.4~1, suggesting the characteristic mesoporous structure.[21] The pore size of the RGO/NPC is mainly distribute between 1~5 nm, which exhibits broad pore size distributions in the micro- and mesoranges (Fig. 3b) with a specific surface area of 65.0 m^2 g^{-1}, and thus confirms the hierarchically porous structure of the RGO/NPC. The hierarchical porous structure would offer more favorable storage sites for the Na^+, while the large surface area provides Na^+ with more adsorption sites. [22]

The XPS spectra (Fig. 4) are used to confirm the N-doped of the RGO/NPC composite. In the XPS spectrum (inset of Fig. 4a), the peaks center at 284.4, 400.6, and 532.1 eV correspond to C 1s of sp^2 C, N 1s of the doped N, and O 1s of the absorbed O, respectively, and the atomic percentage of N in the sample is about 10.04 at%. The XPS spectrum of the C 1s (Fig. 4a) can be divided into three peaks, which can be classified into the following bands: C in rings without N at 284.4 eV, C singly bound to O in phenol and ether (i.e. C–OH) at 285.4 eV and C doubly bound to O in ketone and quinine (i.e. N–C=O) at 287.5 eV. In the XPS spectrum of the N 1s (Fig. 5b), four components are observed, suggesting that N atoms are in the four different bonding characters. The N 1s spectrum is divided into three main peaks at 397.7, 398.3, and 400.6 eV, corresponding to pyridinic, pyrrolic/pyridonic, and graphitic nitrogen atoms, respectively. The minor N1s peak at 403.9 eV originates from the N-oxide of pyridinic nirtrogen.[21, 23] Na ions were adsorbed in the pores due to the strong interatomic attraction between the basic pyridinic/pyrrolic N and Na^+. The

graphitic nitrogen bonds with three sp^2 carbon atoms, which is believed to exhibit higher electronegativity (3.04) compared with C (2.55), improving the electronic conductivity of the composite. [24] According to the XPS analysis, it is indicated that the RGO/NPC composite have successfully realized the N-doped.

3.2 Electrochemical performance

Fig 5a displays representative cyclic voltammetry (CV) curves of the RGO/NPC electrode in the range 0.01~3 V. The sharp reduction peak at 0.5 V are due to the electrolyte decomposition and formation of a solid electrolyte interface (SEI) film,[12, 25] which disappear in the following cycles, indicating the reaction to be irreversible. In addition, a pair of redox peaks observed at lower potential (near 0 V), can be assigned to Na^+ insertion into or extration from the carbonaceous materials.[12] In the subsequent cycles, this peak still exists, suggesting the insertion and extraction of the Na^+ is reversible. Notably, the oxidation peak (near 0 V) intensities of the subsequent cycles are stronger than that of the first cycle, this can be explained by Na^+ reaction with N group on the surface accompanied by Na^+ extraction form the composite, similar phenomenon have been reported. [26, 27] After the first cycle, there is reduction peak at around 1.0 V, which is attributed to the reaction between the Na^+ and the surface N group. [12] In the subsequent cycles, this peak still exists, suggesting the reaction to be reversible. Obviously, the second and following CV curves almost overlap, indicating good cycle performance of RGO/NPC.

Fig. 5 (b) exhibits the 1 st, 5 th and 200 th charge-discharge profiles of the RGO/NPC

material within 0.01~3.0 V, at 100 mA g^{-1}. The first charge-discharge cycle reveals the initial discharge and charge capacities to be 615.4 and 180.1 mAh g^{-1}, respectively, exhibiting a 29.3 % initial coulombic efficiency. The large irreversible capacity loss can be results from the electrolyte decomposition and SEI layer forming, coinciding with the results from the CV observations (Fig 5a). In subsequent cycles, the RGO/NPC electrode shows obvious sloping the slope region of the voltage profile and an indistinct plateau (near 0 V)，corresponding to the insertion of sodium between carbon layers and Na^+ absorption into the nanopores by occurring the reaction between the Na^+ and the surface N group, respectively. [28] Notably, the majority of the capacity in our case resulted from sodium insertion between carbon layers and absorption into the nanopores.

The cycle and rate performances of the RGO/NPC electrode were also tested. As seen in Fig. 6a, the CNF/NPC electrode presents a high reversible capacities of 175.9 and 130 mAh g^{-1} at 100 mA g^{-1} and 200 mA g^{-1} after 300 cycles. Discharge capacity becomes relatively stable after ~15 cycles at different rate and the coulombic efficiency approaches 100% after several cycles. The small irreversible capacity during each cycle can be explained by the incomplete stabilization of the SEI during the charge-discharge processes.[6]

Fig 6b displays the rate performance of the RGO/NPC electrode. This electrode can deliver the initial reversible capacities of 557.1, 165.4, 115.7 and 104 mAh g^{-1} at the current rates of 50, 100, 800 and 1600 mA g^{-1}, respectively. While cycling at a current density as high as 1600 mA g^{-1}, a capacity of 104 mAh g^{-1} can still be reserved.

When the rate is lowered back to 200 mA g^{-1}, the capacity recovers to 149.5 mAh g^{-1}. The results demonstrate that the RGO/NPC electrode exhibits a high rate capability and structural stability even at different Na^+ insertion-extraction velocities.

Figure 5c shows the cyclability of the RGO/NPC electrode at a constant current density of 1000 mA g^{-1}. After ~30 cycles, the specific capacity stay around 100 mAh g^{-1}, and a high coulombic efficiency (approaches 100%) is obtained. After 500 cycles, the electrode can even retains a reversible capacity of 97.7 mAh g^{-1} with tiny decay.

Based on existing research, [29] the nitrogen-free RGO prepared by heat treatment of GO deliver a capacity of 54 mAh g^{-1}, at 50 mA g^{-1} after 55 cycles, which is much lower than that of RGO/NPC electrode. The good electrochemical performance may attribute to the synergies of the fine and uniform NPC and 2D RGO nanosheets.

The favourable electrochemical performance of this RGO/NPC anode for SIBs can be contributed to the several reasons: (1) large interlayer spacing (0.36 nm) of the structured of RGO/NPC, which also can make Na^+ insert into/extract from the carbonaceous anode; (2) the NPC with the appropriate N-doped, which can enhance the electric conductivity, react with the Na^+ and absorb Na^+ into the nanopores; (3) the existence of 2D RGO nanosheets provide high electronic conductivity; (4) high surface area and hierarchical porous structure, which provide Na^+ conductive pathways and adequately contact with the electrolyte.

4. Conclusion

Graphene/nitrogen-doped porous carbon nanofiber (RGO/NPC) composite was successfully synthesized by carbonizing reduced graphene oxide /polyprrole nanofiber

(GO/PPy) precursor. A microstructure of fine and uniform porous carbon nanofiber decorated on 2D RGO sheets was obtained. Nitrogen-doped porous carbon nanofiber can provide large interlayer spacing, appropriate N-doped and hierarchical porous structure to improve the reversible specific capacity. 2D RGO nanosheets provide faster electron transfer channels. Combing the fine and uniform NPC with 2D RGO nanosheets, the RGO/NPC composite displays a excellent rate capability (104 mAh g^{-1} at 1600 mA g^{-1}) and superior cycling stability (97.7 mAh g^{-1} at1000 mA g-1 over 600 cycles), which proving its novelty and importance as an anode for the sodium-ion batteries.

Acknowledgement

The authors acknowledge the financial support of the Teacher Research Fund of Central South University (2013JSJJ027). This project was supported by Grants from the Project of Innovation-driven Plan in Central South University (2015CXS018) and supported by State Key Laboratory of Powder Metallurgy, Central South University, Changsha, China.

Notes and reference

1. B. Scrosati and J. Garche, *Journal of Power Sources*, 2010, **195**, 2419-2430.
2. T. Kennedy, E. Mullane, H. Geaney, M. Osiak, C. O'Dwyer and K. M. Ryan, Nano letters, 2014, 14, 716-723.
3. M. D. Slater, D. Kim, E. Lee and C. S. Johnson, *Advanced Functional Materials*, 2013, **23**,

947-958.

4. S. Y. Hong, Y. Kim, Y. Park, A. Choi, N.-S. Choi and K. T. Lee, *Energy & Environmental Science*, 2013, **6**, 2067.
5. J. Sangster, *Journal of Phase Equilibria and Diffusion*, 2007, **28**, 571-579.
6. K. Tang, L. Fu, R. J. White, L. Yu, M.-M. Titirici, M. Antonietti and J. Maier, *Advanced Energy Materials*, 2012, **2**, 873-877.
7. Y. X. Wang, S. L. Chou, H. K. Liu and S. X. Dou, *Carbon*, 2013, **57**, 202-208.
8. A. Rudola, K. Saravanan, C. W. Mason and P. Balaya, *Journal of Materials Chemistry A*, 2013, **1**, 2653.
9. X. Li, M. M. Hasan, A. L. Hector and J. R. Owen, *Journal of Materials Chemistry A*, 2013, **1**, 6441.
10. W. Li, S. L. Chou, J. Z. Wang, J. H. Kim, H. K. Liu and S. X. Dou, *Advanced materials*, 2014, **26**, 4037-4042.
11. X. Zhou and Y. G. Guo, *ChemElectroChem*, 2014, **1**, 83-86.
12. Z. Wang, L. Qie, L. Yuan, W. Zhang, X. Hu and Y. Huang, *Carbon*, 2013, **55**, 328-334.
13. Y. Bai, Z. Wang, C. Wu, R. Xu, F. Wu, Y. Liu, H. Li, Y. Li, J. Lu and K. Amine, *ACS applied materials & interfaces*, 2015, **7**, 5598-5604.
14. X. Huang, X. Qi, F. Boey and H. Zhang, *Chemical Society reviews*, 2012, **41**, 666-686.
15. D. J. Xue, S. Xin, Y. Yan, K. C. Jiang, Y. X. Yin, Y. G. Guo and L. J. Wan, J*ournal of the American Chemical Society*, 2012, **134**, 2512-2515.
16. W. H. Shin, H. M. Jeong, B. G. Kim, J. K. Kang and J. W. Choi, *Nano letters*, 2012, **12**, 2283-2288.

17. G. Lota, K. Fic and E. Frackowiak, *Energy & Environmental Science*, 2011, **4**, 1592.

18. H. G. Wang, Z. Wu, F. L. Meng, D. L. Ma, X. L. Huang, L. M. Wang and X. B. Zhang, *ChemSusChem*, 2013, **6**, 56-60.

19. S. Li, K. Shu, C. Zhao, C. Wang, Z. Guo, G. Wallace and H. K. Liu, *ACS applied materials & interfaces*, 2014, **6**, 16679-16686.

20 Y. Xu, H. Bai, G. Lu, C. Li and G. F. Shi, *Journal of the American Chemical Society*, 2008, **130**, 5856–5857.

21. Q. Li, Z. Zhang, Z. Guo, Y. Lai, K. Zhang and J. Li, *Carbon*, 2014, **78**, 1-9.

22. Y. Yan, Y.-X. Yin, Y.-G. Guo and L.-J. Wan, *Advanced Energy Materials*, 2014, **4**, 1301584.

23. W. Chen, Z. Zhang, Q. Li, Y. Lai and J. Li, *ChemElectroChem*, 2015, **2**, 246-252.

24. F. Sun, J. Wang, H. Chen, W. Li, W. Qiao, D. Long and L. Ling, *ACS applied materials & interfaces*, 2013, **5**, 5630–5638

25. L. Fu, K. Tang, K. Song, P. A. van Aken, Y. Yu and J. Maier, *Nanoscale*, 2014, **6**, 1384-1389.

26. S. Wenzel, T. Hara, J. Janek, and P. Adelhelm, *Energy & Environmental Science*, 2011, **4**, 3342-3345.

27. C. Li, X. Yin, L. Chen, Q. Li and T. Wang, *Journal of Physical Chemistry C*, 2009, **113**, 13438-13442.

28. Y. Matsumura, S. Wang and J. Mondori, *Journal of The Electrochemical Society*, 1995, **142**, 2914-2918.

29. F. Yang, Z. Zhang, K. Du, X. Zhao, W. Chen, Y. Lai and J. Li, *Carbon*, 2015, **91**,88-95.

Figures and figure captions

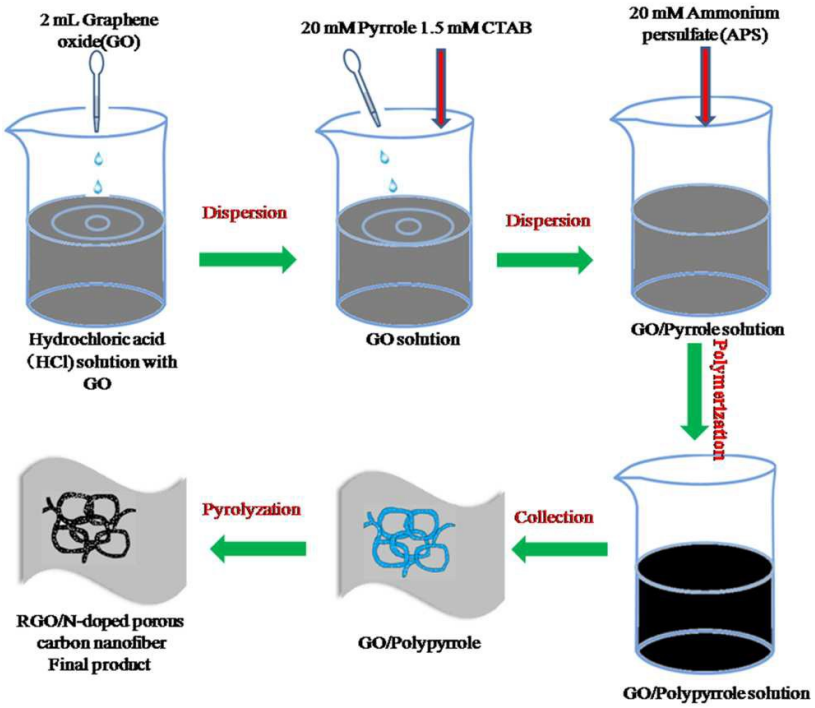

Fig. 1 Schematic of the RGO/NPC fabricate procedure.

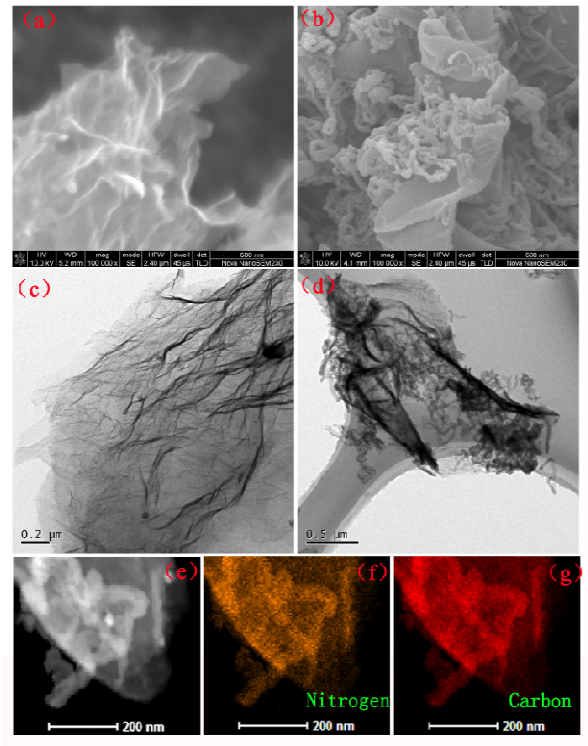

Fig. 2 SEM images of (a) graphene (RGO), (b) graphene/nitrogen-doped porous carbon nanofiber (RGO/NPC). TEM image of (c) RGO, (d) RGO/NPC. (e) Annular dark-field TEM image, and corresponding (f) nitrogen and (g) carbon elemental mapping of RGO/NPC .

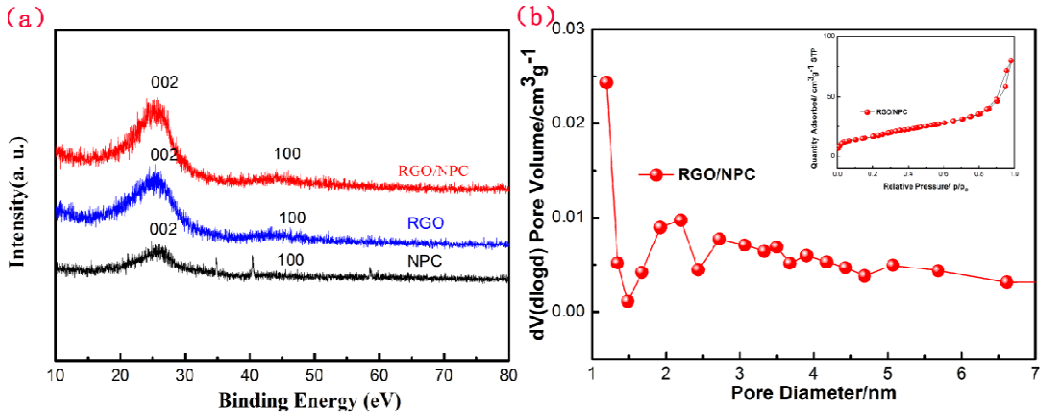

Fig. 3(a) XRD pattern of the RGO, NPC and RGO/NPC. (b) The pore size distribution of RGO/NPC, the inset picture displays N2 adsorption–desorption isotherms.

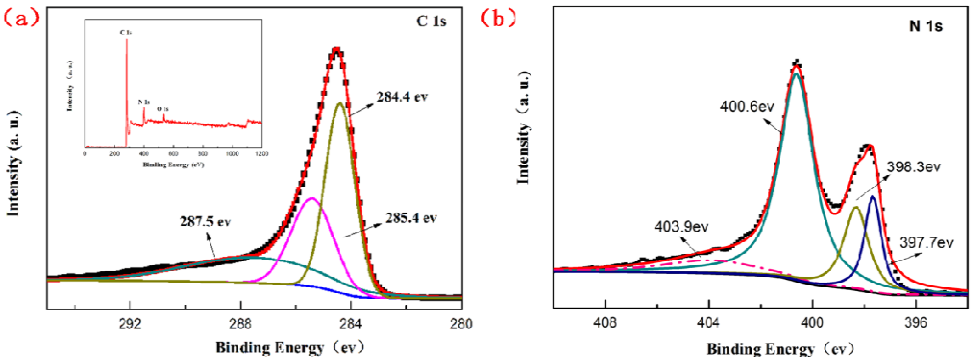

Fig. 4 (a) the XPS C 1s spectra of RGO/NPC, the inset picture is the XPS spectrum of RGO/NPC. (b) The XPS N 1s spectra of the RGO/NPC.

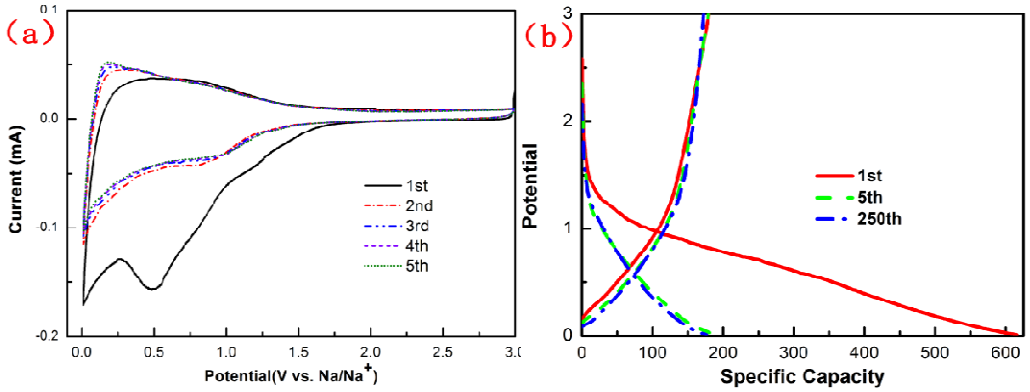

Fig. 5(a) Typical CV curves of the RGO/NPC electrode at a potential sweep rate of 0.2 mV s^{-1} and (b) The 1st, 5th and 200th charge-discharge profiles of the RGO/NPC at 100 mA g^{-1}.

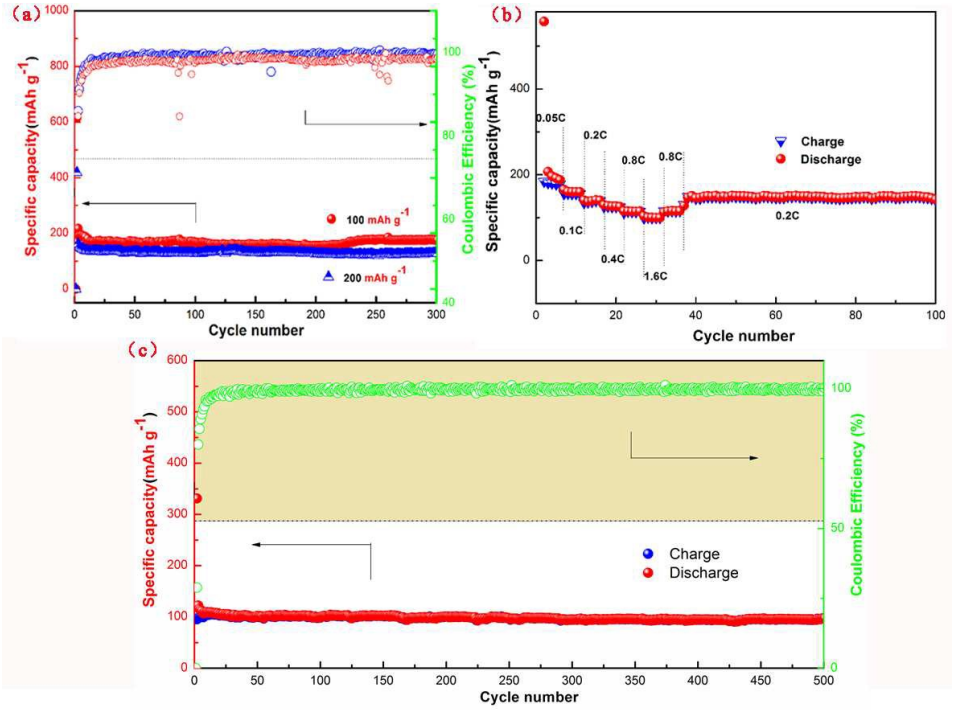

Fig. 6 (a) Cycle performances at current density 100 mA g^{-1} and 200 mA g^{-1} of the RGO/NPC electrode. (b) Rate performance of the RGO/NPC anode electrode. (c) Long cycle performance at 1000 mA g^{-1} of the RGO/NPC anode electrode.

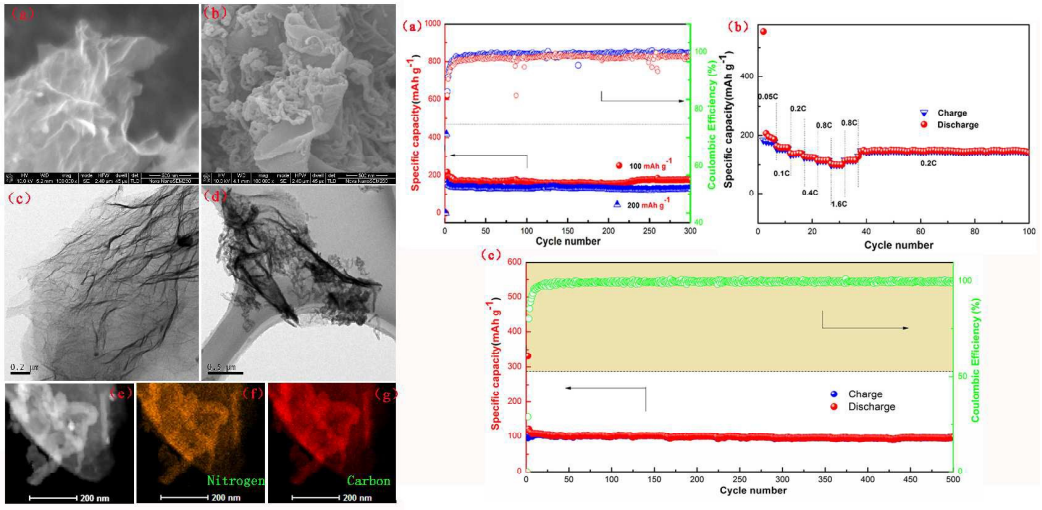

Graphene/N-doped porous carbon nanofiber (RGO/NPC) composite was designed as an anode material for sodium-ion batteries (SIBs). A microstructure of fine and uniform N-doped porous carbon nanofibers decorated on 2D RGO sheets was obtained. Unique compositional and structural features endow the RGO/NPC with superior SIBs performance, that is, an excellent rate capability (104 mAh g^{-1} at 1600 mA g^{-1}) and superior cycling stability (97.7 mAh g^{-1} at 1000 mA g^{-1} over 600 cycles).